Nonlocal electron-phonon coupling in prototypical molecular semiconductors from first principles

Xiaoyu Xie,[†,‡] Alejandro Santana-Bonilla,[†] and Alessandro Troisi[*,†]

†*Department of Chemistry, University of Liverpool, Liverpool L69 3BX, UK*

‡*School of Chemistry and Chemical Engineering, Nanjing University, Nanjing 210023, China*

E-mail: A.Troisi@liverpool.ac.uk

Abstract

A substantial amount of evidence indicates a relevant role played by the nonlocal electron-phonon couplings in the mechanism of charge transport in organic semiconductors. In this work, we compute the nonlocal electron-phonon coupling for the prototypical molecular semiconductors rubrene and tetracene using the phonon modes obtained from *ab initio* methods. We do not make the rigid molecular approximation allowing a mixing of intra- and intermolecular modes and we use a supercell approach to sample the momentum space. Indeed, we find that some low-frequency intramolecular modes are mixed with the rigid-molecule translations and rotations in the modes with the strongest electron-phonon coupling. To rationalize the results we propose a convenient decomposition of the delocalized lattice modes into molecular-based modes.

1 Introduction

There is now overwhelming evidence that the charge mobility in molecular semiconductor is limited by the coupling of the carrier with low frequency phonon through nonlocal electron-phonon coupling, i.e. the modulation of the transfer integral between nearest neighbours due to large amplitude molecular motions.[1–3] The proposed role of nonlocal electron-phonon coupling dates back to the 70s[4] and was reconsidered a number of times in the context of band transport (in Boltzman transport theory[5] phonons are responsible of the carrier scattering) or band renormalization theory,[6,7] i.e. where the coupling with the phonons decreases the band-width slowing down the carrier which would acquire a larger effective mass. The mathematical details of band renormalization theory due to nonlocal electron-phonon coupling are relatively involved but, ultimately, this way of accounting for the nonlocal coupling does not alter the mechanism of transport: delocalised carrier in (polaronic) band are expected to be scattered (infrequently) by impurities. This idea is challenged in two different ways. If one considers a good molecular semiconductor with mobility $\mu \simeq 1$ cm^2/(V·s) at room temperature it is possible to work out the mean free path for the carrier in a band which should be typically of the order of few Angstroms, i.e. too short for a delocalised transport picture and beyond the Ioffe-Regel criterion.[8] Another important insight, derived from coupled classical molecular dynamics and quantum chemistry simulations, is that the collective effect of the low frequency modes is to generate a modulation of the transfer integral of amplitudes comparable to the transfer integral itself and of timescale of the order of $\simeq 1$ ps, comparable with the timescale of carrier dynamics.[7,9,10] This is conveniently termed "dynamic disorder" because of the little correlation observed in the fluctuation of the transfer integrals.[1]

Many theoretical works have attempted a description of this highly coupled charge-phonon dynamics involving methods developed in chemical physics and solid state physics and including Erhenfest dynamics[11] and modified surface hopping[12,13] on model Hamiltonian[14–17] or realistic chemical models.[18,19] All these models suggest that the effect of dynamic disorder is to cause dynamic localisation, i.e. the instantaneous eigenstates of the system are

localised but the dynamic nature of the disorder itself promotes propagation of the charge. An intuitive yet quantitative picture was proposed by Fratini and co-worker, according to which the charge diffusivity is the ratio between a squared "transient localisation" and a characteristic time for the charge to be localised.[8]

Somewhat encouraged by these theoretical proposals a number of experimental groups started developing methodologies to characterise and control the dynamic disorder, because, regardless of the detail of the theory, reducing disorder is expected to increase the mobility. The team in Cambridge has pioneered a new technique to evaluate the large amplitude motions of molecular semiconductors in situ via electron diffraction[20] and rationalised the higher performance of semiconductors on the basis of reduced dynamic disorder.[21] The team led by Takeya has proposed that a suitable mechanical deformation of molecular films can improve their performances by controlling the amount of dynamic disorder.[22] These methods nicely complement the data on molecular crystal vibration traditionally obtained via Raman spectroscopy.[23] Currently there are no design principles for molecules or materials to display the smallest possible amount of nonlocal electron-phonon coupling and, in many of the theories, the effect of disorder is understood as a cumulative effect of many low frequency modes. Analysing the nonlocal electron-phonon coupling in detail, mode by mode (as done in the early works[24]), can reveal interesting chemical patterns and possibly even suggest new chemical design rules for materials insensitive to disorder. The phonon modes in semiconducting crystals have been traditionally computed under the rigid-body approximation,[25] i.e. assuming that intramolecular restoring forces are stronger in comparison with the deformation forces exerted on each molecule by the weak van der Waals (vdW) intermolecular interactions.[26] The main advantage of this assumption is to offer a convenient physical picture in which an effective separation between the internal (molecular vibrations) and external (acoustic and intermolecular translations and librations) degrees of freedom can be carried out.[10]

However, this is a significant hindrance to an accurate description of the electron-phonon

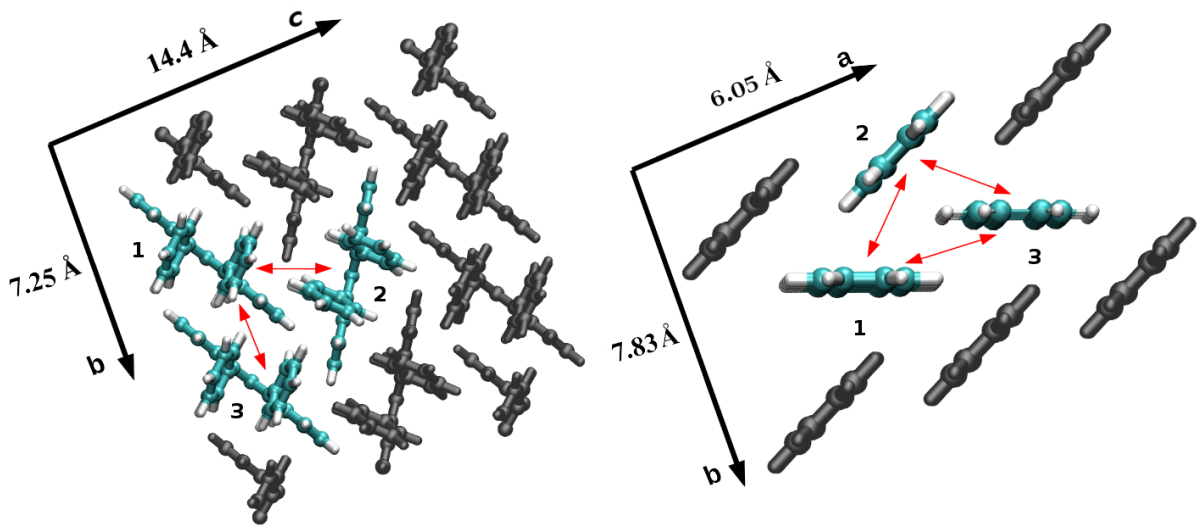

(a) (b)

Figure 1: The crystal structure and lattice parameters within the (a) *bc* layer of rubrene and (b) *ab* layer of tetracene unit cells. In both cases we highlight the symmetry inequivalent molecular pairs for which the electron transfer integrals are computed (red arrows).

coupling at low frequency, where the strength of the nonlocal electron-phonon coupling is affected by the hybridization of intra- and inter- molecular vibration modes.[27,28]

The aim of this work is to study the nonlocal electron-phonon coupling in two prototypical systems (see Figure (1)), tetracene (chosen for its simplicity and small size) and rubrene (one of the best performing molecular semiconductor – with a fairly large unit cell) using phonons obtained from quantum chemical methods.[29,30] We adopt a methodology that is relatively fast (to be potentially translated into a materials discovery tool) but (i) able to deal with the growing diversity of the chemical space currently explored, unlike the classical force field used earlier, and (ii) able to incorporate the effect of dispersion interactions, which limited the effectiveness of simple DFT methodologies until few years ago. We explore aspects such as the importance of sampling the q -space, the relative importance of acoustic and optical modes and their possible mixing, the identification of specific modes with high electron-phonon coupling and useful rationalisation of the results.

2 Method and computational details

2.1 Model Hamiltonian

A tight-binding Hamiltonian for the study of charge transport in molecular semiconductors can be written as:

$$\hat{H} = \hat{H}_{el} + \hat{H}_{ph} + \hat{H}_{el-ph} \tag{1}$$

the electronic part of the Hamiltonian is:

$$\hat{H}_{el} = \sum_{i} \varepsilon_i^0 \hat{a}_i^\dagger \hat{a}_i + \sum_{i \neq j} t_{ij}^0 \hat{a}_i^\dagger \hat{a}_j \tag{2}$$

where i and j indexes indicate molecular orbitals localised on the corresponding molecule (e.g. the HOMOs for hole transport), ε_i^0 and t_{ij}^0 represent the on-site electronic energy and the transfer integral terms; $\hat{a}_i^\dagger(\hat{a}_i)$ are the creation (annihilation) electron operators. The transfer integrals have non-zero value only between molecules in contact. The phonon term is described by:

$$\hat{H}_{ph} = \sum_{I} \hbar\omega_I (\hat{b}_I^\dagger \hat{b}_I + \frac{1}{2}) \tag{3}$$

where $\hat{b}_i^\dagger(\hat{b}_i)$ are creation (annihilation) phonon operators. In this case, the label I incorporates the continuous wavevector q and the phonon branch λ along with the corresponding phonon frequencies ω_I.

The force constant matrices can also be represented in the Fourier space (dynamical matrices) whence the dependence of the phonon frequency (ω) on the wavevector (q) can be computed (phonon-dispersion relations). Lastly, the electron-phonon interaction part is expressed as:

$$\hat{H}_{el-ph} = \sum_{i,I} g_i^I (\hat{b}_I^\dagger + \hat{b}_I)\hat{a}_i^\dagger \hat{a}_i + \sum_{i \neq j,I} g_{ij}^I (\hat{b}_I^\dagger + \hat{b}_I)\hat{a}_i^\dagger \hat{a}_j \tag{4}$$

where the coupling term consists of the electron and phonon operators linked by the electron-phonon coupling. The total electron-phonon coupling is explicitly separated in terms of the local (g_i^I) and the nonlocal (g_{ij}^I) contributions.[3] These two terms represent different physical pictures in which either the predominantly intramolecular (local) or the predominantly intermolecular (nonlocal) vibrations couple to the electronic states participating in the transport phenomena. The transfer integral between two electronic states (defined as $|i\rangle$ and $|j\rangle$) can be recast as,

$$t_{ij} = \langle i|\hat{H}|j\rangle = t_{ij}^0 + \sum_I g_{ij}^I Q_I \tag{5}$$

where Q_I is the dimensionless coordinate of the associated normal mode.[25] Finally, it is worth noticing that to create a link between the general Hamiltonian and the computational method, the electronic operators are expressed in the basis of localized molecular orbitals while the phonon operators are in the basis of the (delocalized) system phonons.

2.2 Computational details

In this work, the interatomic forces have been calculated by employing the self-consistent-charge density-functional tight-binding (SCC-DFTB) method as implemented in the DFTB+ software package.[29–32] The DFTB semi-empirical method can be described as an intermediate step between a simple parametrized tight-binding model and a fully *ab initio* density functional theory (DFT) making it a very efficient methodology to compute electronic and mechanical properties of large systems while preserving quantum mechanical effects.[33] In the case of the electronic structure calculations, the diagonal elements of the resulting general tight-binding Hamiltonian matrix are chosen to be self-consistent atomic DFT eigenvalues evaluated with the PBE exchange-correlation functional, while the off-diagonal elements are

calculated in a two-center approximation as is the case of the employed 3-ob-1 Slater-Koster set parameter.[33,34] In order to characterise the weakly vdW interactions responsible of the intermolecular interactions in the crystalline phases the recently developed DFTB-D3 formalism is employed[35,36] in which the Coulomb interaction between atomic partial charges is improved by expanding in a Taylor series the exchange-correlation energy functional up to third order correction in order to include the charge dependence of the Hubbard parameter.[37] The atomic positions of the unit cell using periodic boundary conditions (PBC) are optimized keeping the experimental lattice values fixed. The conjugate gradient method has been used with a force-threshold criterion of 10^{-6} Hartree per Bohr radius.

In connection with the solution of the electronic tight-binding Hamiltonian, the Hessian matrix is computed at the obtained relaxed geometry where the corresponding harmonic normal modes of the unit cell at Γ-point are calculated by diagonalizing the mass-weighted Hessian. In order to test the accuracy of our methodology for the gas-phase molecules, we have computed the electronic (energy level splittings) and mechanical properties (vibrational frequencies) of tetracene and rubrene with DFTB+ and compare the obtained results with the ones calculated from the all-electron first-principle calculations as implemented in the Gaussian 09 software.[38–40] Based on the results obtained from this procedure and shown in the ESI, we can conclude that DFTB+ delivers reliable results to describe the mechanical properties of the aforementioed systems.

To investigate the phonon dispersion relations in crystalline phases, we have employed the frozen phonon calculation in which the sampling of the q-space relies on calculation of second derivatives of the energy on sufficiently large supercells.[41–43] Consequently, we have found that a supercell size of $2 \times 2 \times 2$ is necessary to describe all normal modes for tetracene while for rubrene a supercell size of $1 \times 4 \times 2$ is required. These calculations have been carried employing a $1 \times 1 \times 1$ k-point sampling Monkhorst-Pack scheme. The aforementioed supercells yield converged phonon band structure in which no noticeable changes are observed.[44] The accuracy of this methodology has been contrasted in the case of tetracene

crystal by comparing with the reported results in literature and calculations obtained by Density Functional Perturbation Theory (DFPT) as implemented in the Quantum-Espresso package validating the use of DFTB+ to describe the mechanical properties in these materials (a detailed discussion and the corresponding phonon band structures are displayed in the ESI).[45,46]

The transfer integral between neighbouring molecular pairs was computed from calculations of isolated dimers. The Kohn-Sham total Hamiltonian for these systems is calculated by employing an orthonormalised atomic basis set. The block-diagonal methodology has been used to construct the diabatic Hamiltonian in terms of the selected localized molecular orbitals by correctly transforming the Fock matrix extracted from adiabatic first-principle calculations.[47] Thus, the off-diagonal terms of the transformed Hamiltonian are the desired charge-carrier transfer integrals and computed as:

$$t_{ij} = \langle i|\hat{\mathbf{F}}|j\rangle \tag{6}$$

where $\hat{\mathbf{F}}$ is the Fock operator of the dimer system and $|i\rangle$, $|j\rangle$ represent the molecular orbitals localised on molecule i and j, respectively. Throughout this study the transfer integrals of tetracene and rubrene organic semiconductors are computed by employing the localised highest-occupied molecular orbitals (HOMO) of each moiety at the studied molecular-pair. Calculations of the transfer integrals are carried out performing *ab initio* calculations at the B3LYP/6-31G* level of theory as implemented in Gaussian 09.[40]

According to Eq. 5, the nonlocal electron-phonon coupling due to mode I and for molecular pair ij can be expressed as:

$$g_{ij}^{I} = \frac{\partial t_{ij}}{\partial Q_I} \tag{7}$$

To evaluate efficiently the derivative in Eq. 7 we represent the mode as a vector of Cartesian displacements $\mathbf{Q}_I^c = \{x_k^I\}$. The Cartesian gradient of the transfer integral can be

defined as $\nabla t_{ij} = \{\frac{\partial t_{ij}}{\partial x_k}\}$ (the elements of this vector are zero if displacements x_k are not of the molecules i or j). The electron phonon coupling can be then computed as:

$$g_{ij}^{I} = \nabla t_{ij} \cdot \mathbf{Q}_{I}^{c} \tag{8}$$

This formulation is useful because the first term of the product does not depend on the phonons and only includes a limited number of differentiation ($6N_a$ where N_a is the number of atoms in one molecule) while the second term does not depend on the electronic coupling. To evaluate ∇t_{ij}, a range of displacements from -0.01 Å to 0.01 Å for each component of the gradient and a five-point numerical derivative scheme have been employed.

3 Results and Discussion

3.1 Phonon dispersion

The underlying lattice environment of each molecular crystal defines not only the moiety packing but also the nature of the participating phonons in which the charge carrier transfer process occurs. Modes with frequency higher than 200 cm^{-1} are typically intramolecular, have modest dispersion, and can be conveniently and effectively described from gas phased calculations. The low frequency phonons are expected to be the ones with the strongest nonlocal electron-phonon coupling and for which a strong mixture between intra- and inter-molecular modes can be anticipated. Therefore, to study the behaviour of these modes along the high-symmetry directions where the charge carrier mobility is high the computation of the phonon band structure is necessary.

The results of our calculations (displayed in Figure 2) show a complex phonon spectra for tetracene and rubrene. Firstly, we can observe that in both cases the lowest-lying acoustic branches display an intricated behavior in which a manifold of crossings and anti-crossings of the different phonon bands are observed. In the case of rubrene (Figure 2(a)), because

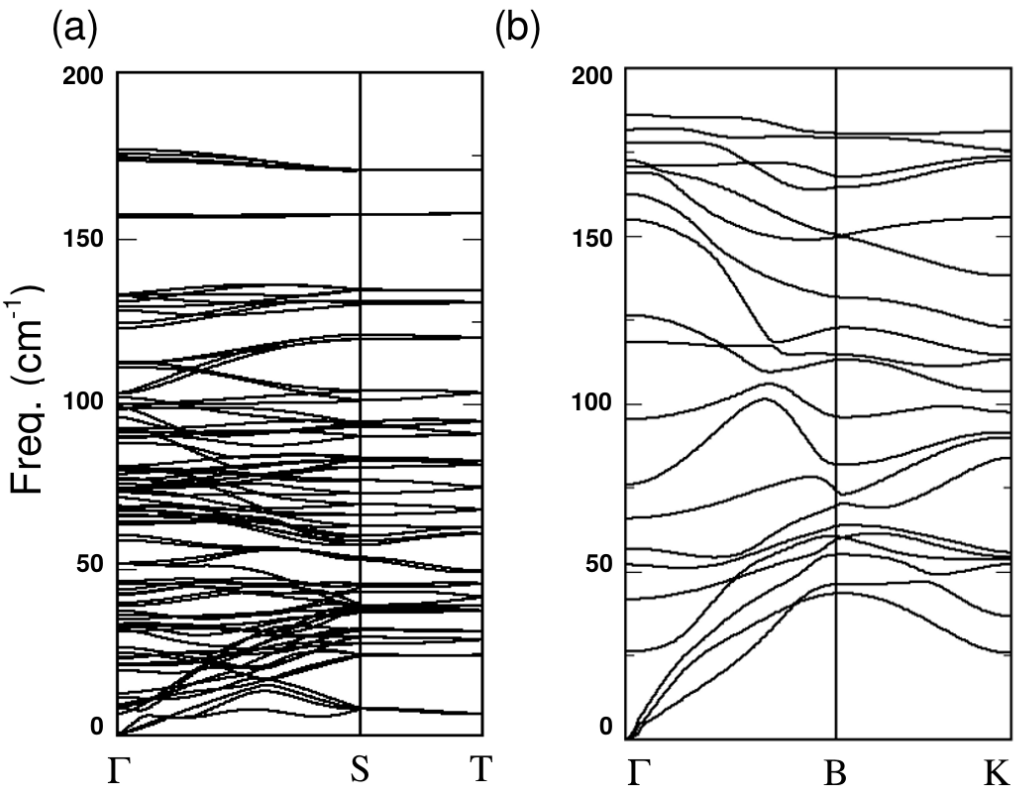

Figure 2: Calculated phonon dispersion shown for (a) rubrene and (b) tetracene molecular crystals along selected high-symmetry points where the charge carrier mobility is high. For rubrene, we selected $\Gamma\,(0,0,0)$, $\mathrm{S}\,(0,0.5,0)$ and $\mathrm{T}\,(0,0.5,0.5)$ high-symmetry points. In the case of tetracene, the depicted points are $\Gamma\,(0,0,0)$, $\mathrm{B}\,(0.5,0,0)$ and $\mathrm{K}\,(0.5,0.5,0)$. The frequency range for both organic semiconductors has been chosen to depict phonon branches whose energy is equivalent to room temperature energy (k_BT).

of the larger number of low frequency modes in the isolated molecule, the lattice (acoustic) and inter-molecular modes are mixed leading to a new combination of atomic collective movements. On the other hand, tetracene phonon spectra (Figure 2(b)) are more easily interpreted because the highest-lying acoustic mode interacts weakly with the first intramolecular accessible modes.

Finally, an important difference between rubrene and tetracene can be observed in terms of the behaviour of the phonon branches along the paths S-T and B-K. For tetracene, the low-frequency phonon branches exhibit dispersion while in rubrene the initial normal modes are merged into bands with almost flat dispersion ascribed to localized modes of vibration in the crystal.

Table 1: HOMO-HOMO transfer integrals (in meV) for tetracene and rubrene selected molecular pairs as shown in Figure 1. Computed values of this work have been compared with previous theoretical calculations[10,26,48,49] and available experimental results.[50,51]

		This work	References			
Tetracene	t_{12}	-76.18	70[50]	-69.5[49]		
	t_{13}	-7.49	-	-5.1[49]		
	t_{23}	25.34	22[50]	17.1[49]		
Rubrene	t_{12}	-18.49	10 ± 15[51]	15[10]	23 ± 10[48]	-6[26]
	t_{13}	102.04	108 ± 4[51]	83[10]	143 ± 51[48]	125[26]

3.2 Analysis of the nonlocal electron-phonon coupling

The magnitude of the equilibrium transfer integrals computed for this work are reported in Table 1 alongside other values found in literature for the same system to display an overall good level of agreement. Note that the sign of the integral between translationally non-equivalent molecules depends on an arbitrary sign of the basis orbital and the sign differences in Table 1 are not significant.

The indexes used in each value of the transfer integral represent the possible combinations between adjacent molecules following the nomenclature introduced in Figure 1. Before discussing the individual contribution to the nonlocal electron-phonon coupling it is convenient to consider the standard deviation (σ^2) as a global measure of the fluctuation of the transfer integrals when compared with their average values. If the vibrations are treated quantum mechanically and thermally averaged this quantity can be computed as:[25]

$$\sigma_{ij}^2 = \frac{1}{N} \sum_I \frac{{g_{ij}^I}^2}{2} \coth\left(\frac{\hbar\omega_I}{2k_BT}\right) \tag{9}$$

where ω_I is the frequency of the normal mode, k_B the Boltzmann constant, T the absolute temperature and N the number of points employed to sample the q-space. Eq. 9 quantifies the relationship between the nonlocal electron$-$phonon coupling and all accessible normal modes statistically weighted by the relative importance of phonon occupation at a given

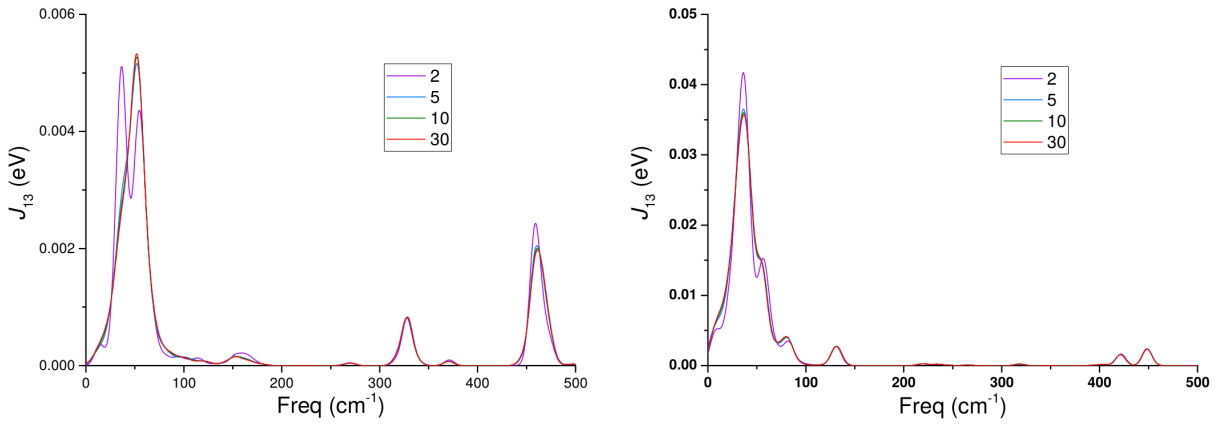

(a) (b)

Figure 3: Spectral densities for (a) tetracene dimer 13 and (b) rubrene dimer 13 (following the nomenclature of Figure 1) with different q-points sampling ($n \times n \times n$).

temperature.

To corroborate the accuracy of this methodology, we have computed the values of the standard deviation (σ^2) for rubrene for molecular pairs 12 ($\sigma_{12} = 9.7$ meV) and 13 ($\sigma_{12} = 49.1$ meV) which are in good agreement to reported values of 9.9 and 50.8 meV, respectively.[48]

Tabular representation is not particularly convenient to appreciate the trends and identify the most important modes coupled to the electron because of the large number of phonon vibrations. We therefore define the spectral density function for the nonlocal electron-phonon coupling as:

$$J_{ij}(\omega) = \frac{1}{2N\hbar} \sum_I {g_{ij}^I}^2 \delta(\omega - \omega_I) \tag{10}$$

where the squared electron-phonon coupling weights the contribution of each mode in the spectrum of frequencies.[52] In the numerical analysis, the δ function has been replaced by a Gaussian distribution with a width of $\sigma = 5$ cm^{-1}.

Because of the large dispersion of the low frequency modes and their role in nonlocal electron-phonon coupling, it is not known a priori how accurately one should sample the reciprocal space to obtain converged results for the spectral density $J_{ij}(\omega)$. We have performed

calculation of the spectral density using a range of sampling of the q-space and report the results in Figure 3. Already with a sampling of $2 \times 2 \times 2$ in the reciprocal space the **J**s are reasonably well described with the results barely changing for sampling beyond $5 \times 5 \times 5$.

The spectral density of symmetry independent molecular pair in the high mobility pair of rubrene and tetracene are reported in Figure (4) and Figure (5), respectively. As a result of the analysis, it is observed that the strongest nonlocal electron-phonon couplings are reported in frequency ranges below 200 cm^{-1} for both systems where in the case of tetracene the most intense component is reported in the J_{12} coupling while for rubrene is reported in the J_{13} component. Likewise, a strong directionality in the strength of the nonlocal electron-phonon coupling is observed in the two cases.

For tetracene, the molecular dimer 12 reports the strongest couplings while in the case of rubrene the nonlocal electron-phonon coupling of the dimer 13 dominates in the low-frequency phonon range of the spectrum. In the case of middle-range phonon frequencies ($200\ \mathrm{cm}^{-1} \leq \omega \leq 1500\ \mathrm{cm}^{-1}$), we observe that some of these normal modes are moderately coupled with the electrons participating in the transport phenomena. This effect is more pronounced in tetracene where more coupled modes are found in comparison with rubrene as can be observed in Figure 4(a,b,c) and Figure 5(a,b).

Analogously, our analysis also suggests that some high-frequency modes also contribute to the total strength of the nonlocal electron-phonon coupling especially in frequency ranges located at $1500\ \mathrm{cm}^{-1} < \omega < 1900\ \mathrm{cm}^{-1}$ for both molecular crystals.

At this point, we now turn to discussing the actual role played by the strength of nonlocal electron-phonon couplings as limiting factor in the charge carrier mobility of organic semiconductors and its influence on the fluctuation of the transfer integral.[3,7,53] In this sense, Eq. 9 offers a suitable theoretical framework to discern the importance of particular set of nonlocal electron-phonon couplings once the effect of thermal population of phonons is included. Thus, for tetracene the 87 % of the computed total variance σ_{ij}^2 (Eq. 9) for all the three investigated dimers can be ascribed to modes whose frequencies are below 200 cm^{-1}.

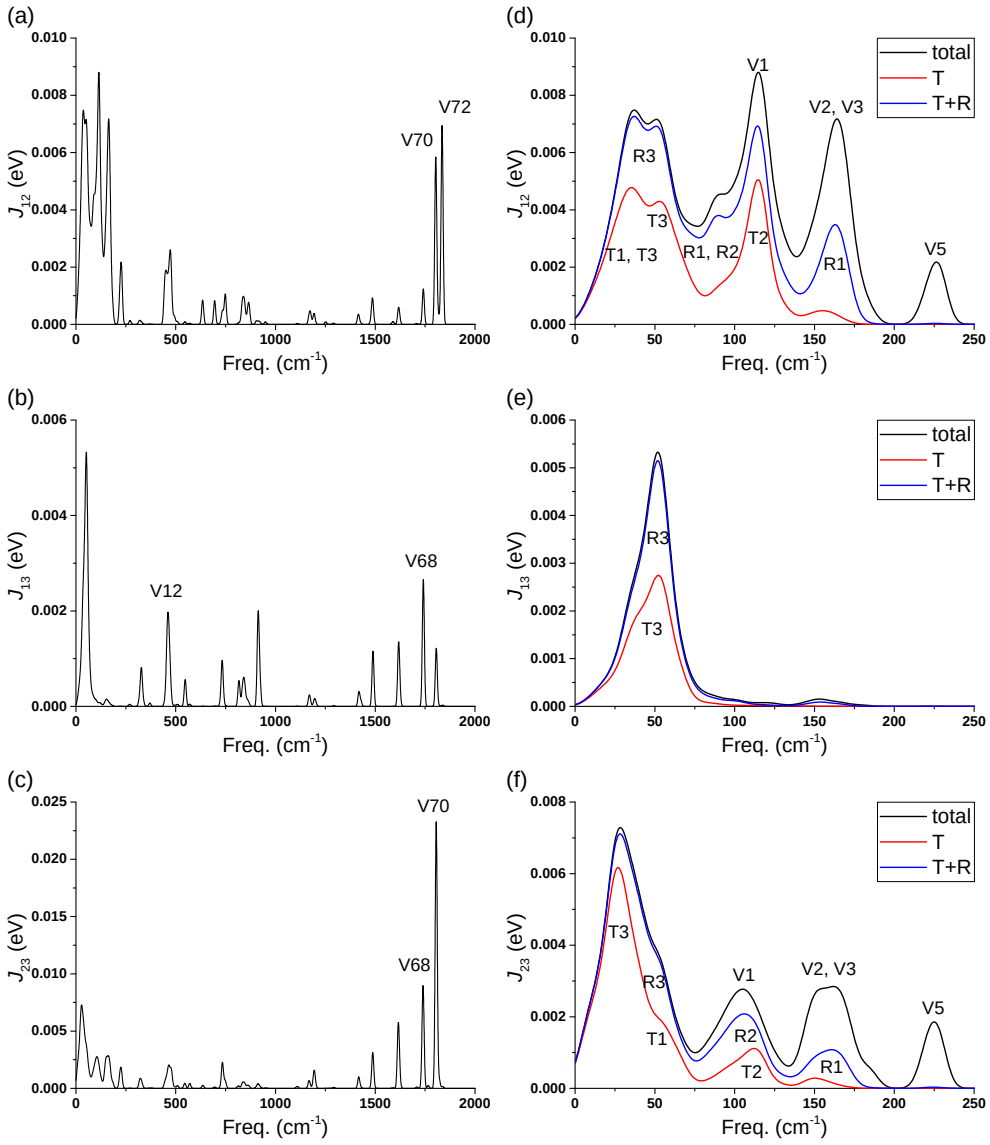

Figure 4: Total spectral density (black line) for dimer 12 (a-b), 13 (c-d) and 23 (e-f) of tetracene. The right panel provides a decomposition of the spectral density in local translation ($T_{1,2,3}$=$\mathbf{l}_1$, $\mathbf{l}_2$, $\mathbf{l}_3$), rotations ($R_{1,2,3}$=$\mathbf{l}_4$, $\mathbf{l}_5$, $\mathbf{l}_6$) and intramolecular vibrations (V_n relate to $\mathbf{l}_{K\geq 7}$) local modes of the monomers in the pair. The label above each peak represents the dominant component of the corresponding vibration.

For rubrene this percentage in both studied molecular pairs is 91 %.

3.3 Local decomposition of the lattice vibrations

A rigorous separation between intramolecular and intermolecular modes can not be carried out with the exception of the three-acoustic modes at the Γ point, corresponding to the

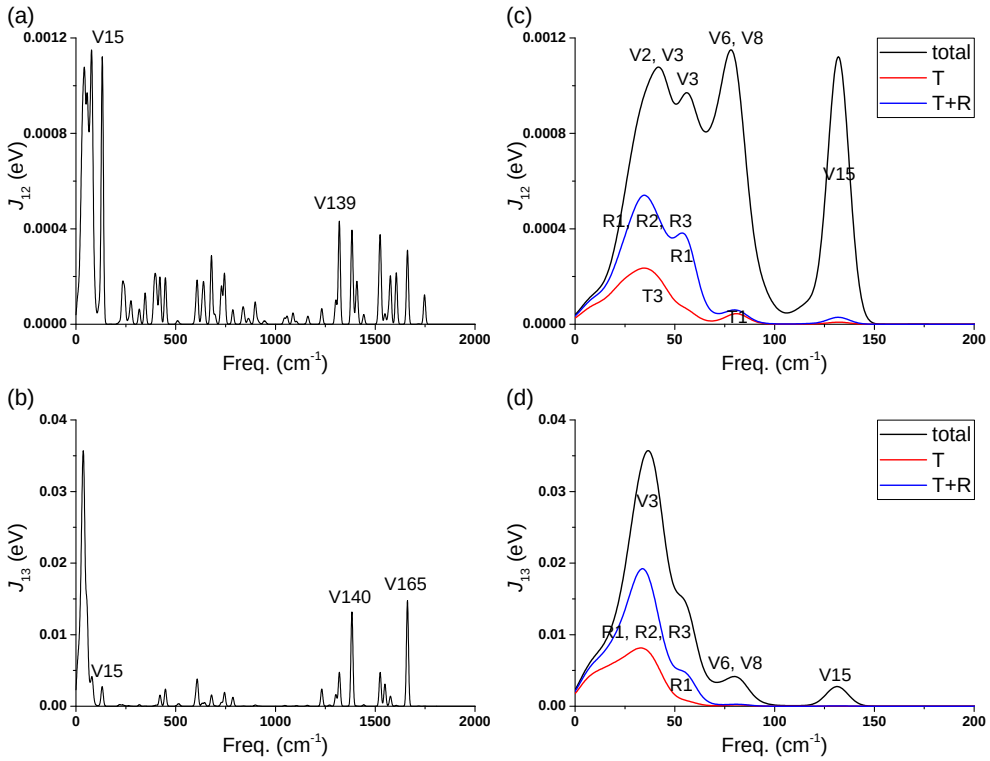

Figure 5: Total spectral density (black line) for dimer 12 (a-b), 13 (c-d) of rubrene. The right panel provides a decomposition of the spectral density in local translation ($T_{1,2,3}$=$\mathbf{l}_1$, $\mathbf{l}_2$, $\mathbf{l}_3$), rotations ($R_{1,2,3}$=$\mathbf{l}_4$, $\mathbf{l}_5$, $\mathbf{l}_6$) and intramolecular vibrations (V_n relate to $\mathbf{l}_{K\geq 7}$) local modes of the indicated monomers in the pair. The label above each peak represents the dominant component of the corresponding vibration.

trivial translation of the crystal. Because of the large number of modes per unit cell and their delocalised nature (especially for low-frequency modes) it is very difficult to visualise the modes that are more strongly coupled with the charge transport.

Since this coupling involves two neighbouring molecules it is useful to devise a projection of the crystal modes into modes localised on a molecular pair to rationalize the nature of the modes associated with large electron-phonon coupling. The molecular dimer is further decomposed in terms of the participating molecular monomers offering a local vibrational basis set. We define a set of molecular modes $\{\mathbf{l}_K^i\}$ localized on molecule i and expressed as mass-weighted Cartesian coordinates where K is the index of the molecular mode. The modes from $K = 7$ to $K = 3N_a$ where N_a is the number of atoms in a molecule, correspond to the vibrational modes of the molecule in gas phase. The modes for $K = 1,\ 2,\ 3$ are the

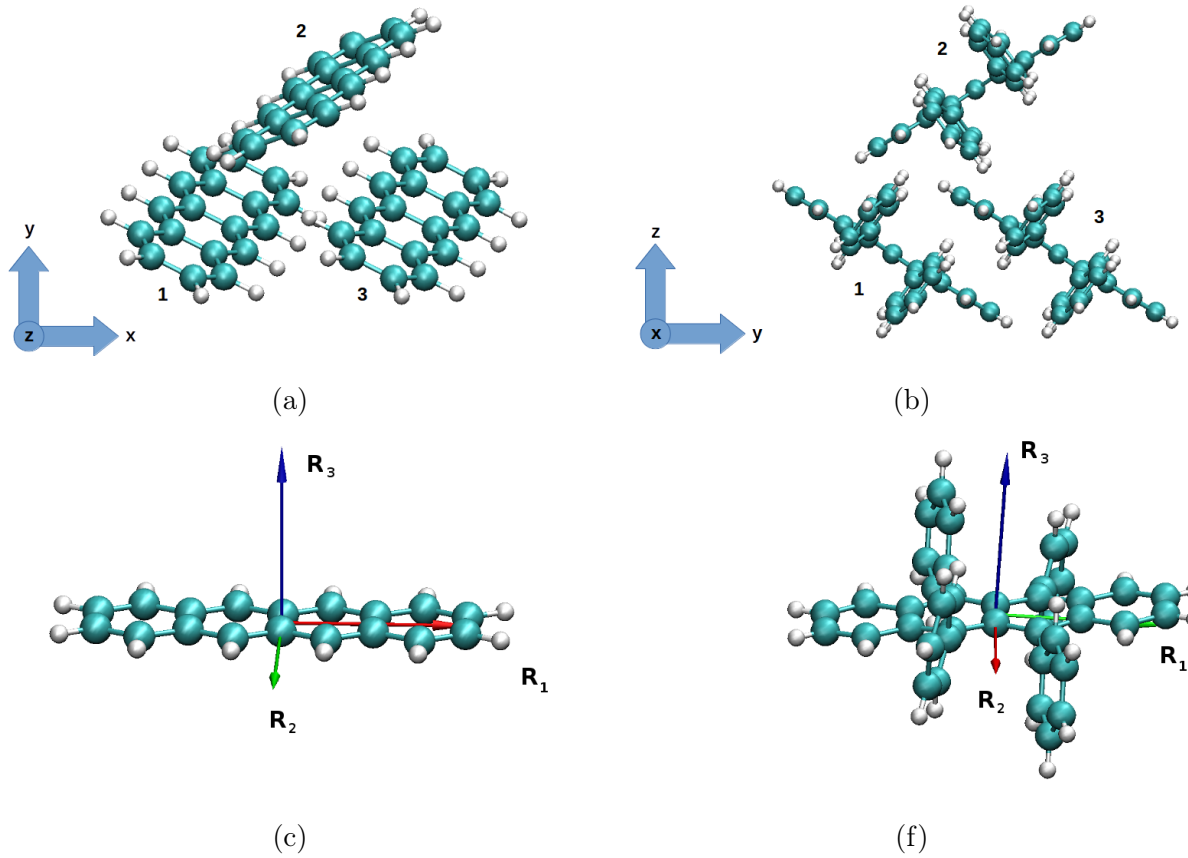

Figure 6: Definition of localised translation and rotation modes for tetracene and rubrene molecular complexes. (a, b) translation modes for tetracene and rubrene, respectively. The labels T_1, T_2 and T_3 are movement of each monomer along x, y and z axes corresponding to $\mathbf{l}^i_{K=1,2,3}$; (c, d) Three molecular rotations (R_1, R_2 and R_3) for the tetracene and rubrene molecule along the three different coordinate axes (indicated by arrows) related to the labels $\mathbf{l}^i_{K=4,5,6}$ (see main text for details of the nomenclature).

translation modes of the rigid molecule and $K = 4,\ 5,\ 6$ are the rotation modes of the rigid molecule. They are defined in Figure 6 for the molecules considered here. Any crystal mode $\mathbf{Q}_I$ (now expressed in mass-weighted Cartesian coordinates) can be projected into each of the localized modes and $(\mathbf{Q}_I \cdot \mathbf{l}^i_K)^2$ is the weight of molecular mode K of molecule i on the crystal mode I. We can therefore decompose the spectral density as sum of molecular mode components as follows (assuming that all modes are normalized):

$$J_{ij}(\omega) = \sum_K J^K_{ij}(\omega) \tag{11}$$

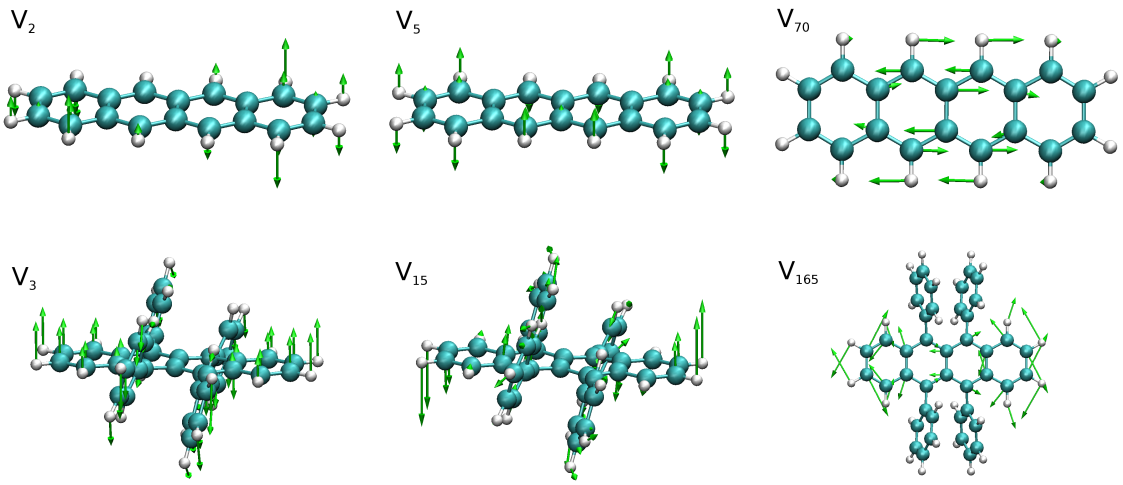

Figure 7: Selected gas-phase molecular vibrations for tetracene (top) and rubrene (bottom) giving a large contribution to the phonons with strongest electron-phonon coupling. The displacements are highlighted by green arrows.

where,

$$J_{ij}^{K}(\omega) = \frac{1}{2N\hbar}\sum_{I}[(\mathbf{Q}_I \cdot \mathbf{l}_K^i)^2 + (\mathbf{Q}_I \cdot \mathbf{l}_K^j)^2] {g_{ij}^I}^2 \delta(\omega - \omega_I) \tag{12}$$

For simplicity we do not distinguish if a mode affecting the coupling between molecule i and j is localized more on one of the two molecules. The first equality is a consequence of the completeness of the subspace of the localized normal modes. At this point we can enrich the plot of the spectral density $J_{ij}(\omega)$ by specifying what fraction of that spectral density derives from a particular group of modes. In the Figures 4(c,d,f) and 5(c,d), we have grouped the components of $J_{ij}(\omega)$ into translation, rotation and all other intramolecular vibration. The definition of the translation and rotational directions used in the present analysis are given in Figure 6 while a representation of selected important modes for the two systems studied here is given in Figure 7.

In the case of tetracene, the rotational (R_2, R_3) and translational (T_3) molecular modes are the predominant contributing modes for frequency ranges below 50 cm^{-1} as shown in Figure 4(d,e,f). Likewise, the projection methodology pinpoints the importance of some particular intramolecular vibrations, particularly strong in the case of rubrene. Indeed, the role played by those modes in the phonon dispersion relation has been a particularly

challenging source of debate due to the lack of an appropriate theoretical framework where those vibrations can be separately studied.[26] As an example, the first important contribution of these low-frequency gas-phase vibrations into the total spectral function in tetracene can be found at frequencies around 120 and 250 cm^{-1} for the molecular pair 12, respectively. A sketch of the atomic movements associated to these vibrations (V_2, V_5) is presented in Figure 7(a, b), where one can observe how these modes display a large out-of-plane deformations of the molecular backbone and where one half of the molecule motion is similar to a computed libration mode (Figure 6(c)).

High frequency modes with strong electron-phonon coupling (like V_{70}) have the character of C-C stretching combination as expected (see Figure 7(c)). In the case of rubrene, intramolecular vibrations contribute more strongly to the low frequency part of the spectral density as shown in Figure 5(c). From the analysis of the spectral density, we know that all three rotations contribute significantly to the total spectral density at frequency ranges below 50 cm^{-1} in combination with the intramolecular mode V_3. The contribution of low-frequency intramolecular modes seen in rubrene but not in tetracene is in part due to the presence of low frequency mode in the isolated rubrene molecule. However, of the five modes of rubrene below 70 cm^{-1} only two display a strong coupling with the carrier. The most important contributions are reported at V_3, V_{15} and V_{165} which are located at frequency regions around 25 cm^{-1}, 125 cm^{-1} and 1600 cm^{-1}, correspondingly. Also here, we observe for the first two modes a large out-of-plane deformation of the molecular backbone. In this case half of the motion depicted in V_3 matches the librational mode displayed in Figure 6(f). The mode V_{15} corresponds to a mirrored version of the atomic motion illustrated in the previously mentioned librational mode, while the mode V_{165} displays a familiar bond stretching patterns as can be observed in Figure 7(f).

In conclusion, the projection onto the isolated molecular modes provides a simple but powerful way to interpret the bare data obtained from the spectral density. A general observed trend in our calculations is that the most strongly coupled modes have the character

of large out-of-plane deformation of particular combination of C-C stretching in the organic core.

3.4 Graphical visualization of strongly coupled modes

The description of the phonon with the largest nonlocal electron-phonon coupling does not reveal any simple pattern and it is maybe not suitable to describe the underlying physical reasons that make a mode more or less strongly coupled to the charge-carrier. A simple analysis can be derived considering the Eq. 8 used to compute the electron-phonon coupling as the scalar product between the gradient of the transfer integral in a molecular dimer (∇t_{ij}) and the phonon displacement ($\mathbf{Q}_I^c$). Analogously, the (squared) scalar product between ∇t_{ij} and the localized molecular modes $\mathbf{l}_K^i$ measure the importance of that mode on the nonlocal electron-phonon coupling. In doing so, we can graphically represent both quantities as a set of arrows centered on the corresponding atoms for the different studied molecular pairs (see Figure 8).

To illustrate this representation for tetracene, the gradient ∇t_{ij} is represented alongside the vibration V_5 on one of the molecules in the 12 pair in Figure 8(a). Thus, one can graphically observe the considerable overlap between the direction of movements of few atoms and direction of the transfer integral gradient, which explains the moderate strength of the electron-phonon coupling in Figure 4(a). Similarly, the projection analysis has been performed onto a high-frequency mode V_{68} on the monomer 1 of the dimer 13 indicating the overlap of the ∇t_{ij} and the displacement of carbon atoms located in the organic-core as is depicted in Figure 8(b). Finally, the strongest nonlocal electron-phonon coupling associated to a high-frequency normal mode is observed in Figure 8(c), where many of the atomic displacements go along with the directionality of the charge transfer.

For rubrene, the projection has been performed onto the low-frequency modes $V_{2,3}$ on the monomer 1 of the isolated dimer 13 where the outcome of the analysis has been plotted in Figure 8(d, e). The results display a strong correlation between several atomic displacements

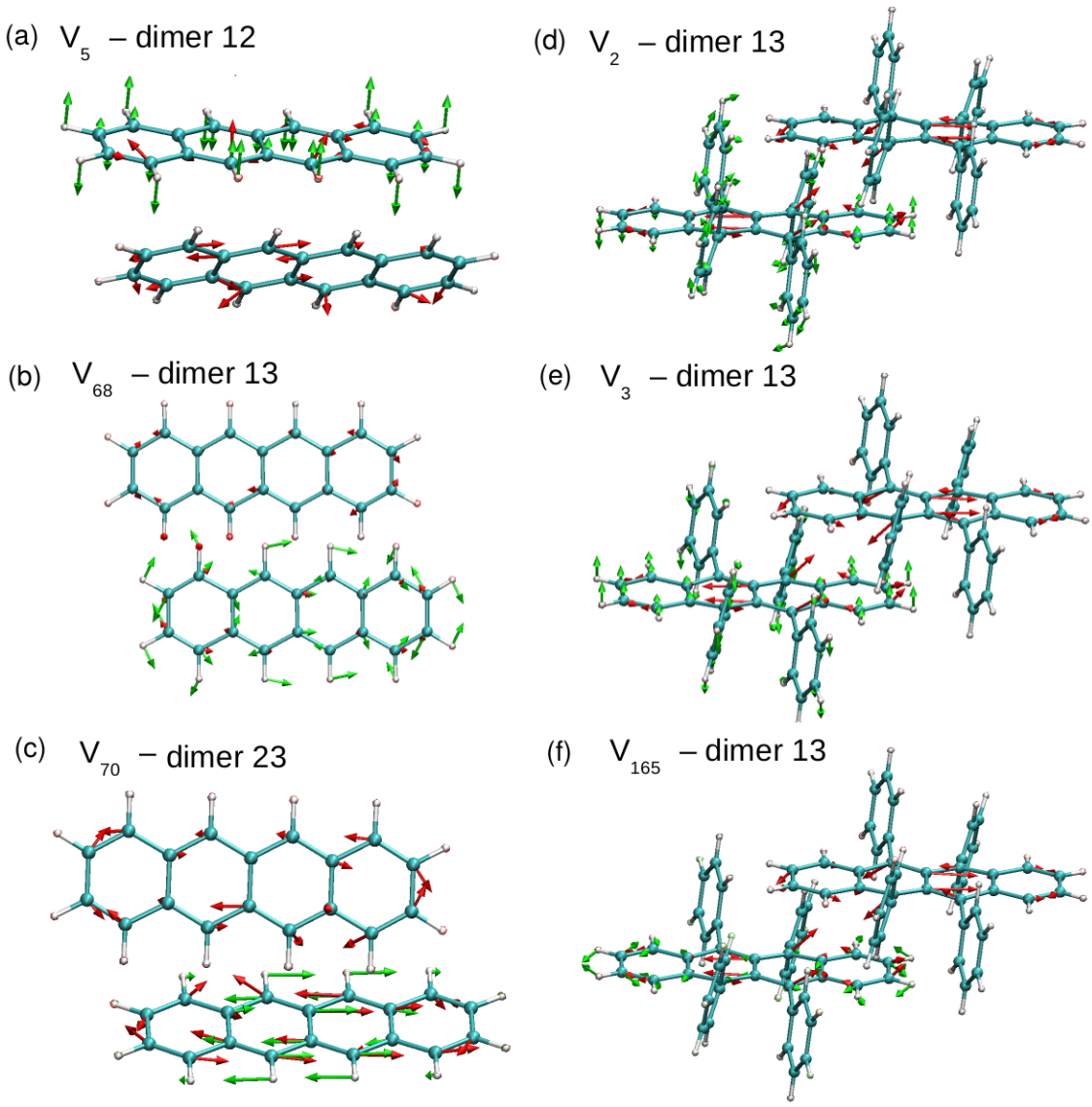

Figure 8: Superposition of the gradient of the transfer integral (red arrows) and green arrows, for modes localised on a single molecule.

with the direction in which the charge transfer is occurring offering a resolved explanation to the large nonlocal electron-phonon coupling reported in Figure 5(b). The high-frequency mode V_{165} has been projected on monomer 1 using the isolated molecular pair 13 (Figure 8(f)). The corresponding atomic displacements along this normal phonon mode and the transfer integral gradient display a poor correlation explaining the reported moderate electron-phonon coupling.

Finally, it has been noted above that the gradient of the transfer integral can be computed relatively quickly, while computing the phonons is expensive especially if a good sampling of the q space is required. If one is interested in computational screening of compounds with a relatively smaller electron phonon coupling, Eq. 8 suggests that it may be convenient to search for the ones with small $|\nabla t_{ij}|$.

4 Conclusions

In conclusion, we have performed a systematic study of the nonlocal electron-phonon coupling employing first-principle calculations of phonons for prototypical semiconductor organic molecular crystals. We found, as anticipated, a very substantial mixing of intra- and intermolecular motions at low frequency, which prevents the accurate evaluation of electron-phonon coupling using a rigid molecule approximation and it is particularly evident for larger molecules such as rubrene. The computation of the nonlocal electron phonon coupling reveals a complex pattern which was interpreted by projecting the phonon modes onto isolated molecule motions. We have found moderate to strong contributions to this coupling from (i) low frequency modes (acoustic modes and librations), (ii) some out of plane modes and (iii) some combination of carbon-carbon stretching modes. When the phonon occupation number is taken into account the strongest contributors to this coupling are the low-frequency modes ($\omega < 200$ cm^{-1}), which are responsible for typically more than 85 % of the fluctuation of the transfer integral at room temperature. The intuitive rationalization of the results remains challenging and, for this reason, we proposed a visualization of the nonlocal electron phonon coupling as the overlap between the gradient of the transfer integral and the normal modes of isolated molecules, which indeed helps explaining all the numerical observations. Our results suggest the possibility to enhance the performance of new materials by targeting two possible strategies. Firstly, one can seek to suppress the amplitude of the normal modes which coincides in the direction of the gradient of the transfer integral leading to an

effective reduction of the nonlocal electron-phonon coupling. For example, by chemical substitution with heavy functional groups that do not alter the packing and electronic structure, as proposed semi-quantitatively in Ref.[21,22] Alternatively, one can promote the formation of molecular motifs where the gradient of the transfer integral between molecules is reduced, using computations like the one presented here to identify such motifs.

Acknowledgement

A.S.B. and A.T. would like to thank EPRSC for financial support. X.X. acknowledges the support of the China Scholarship Council. X.X, A.S.B. and A.T. would like to thank Dr. Daniele Padula, Dr. Tahereh Nematiaram and Mr. Alessandro Landi for fruitful discussions. A.S.B. and A.T. were funded under the embedded CSE programme of the ARCHER UK National Supercomputing Service.

5 Associated Content

The Supporting Information is available free of charge on the ACS Publications website at DOI: XXX.

Validation of DFTB methodology against standard DFT calculations for isolated molecule.

Full phonon band structure for tetracene and rubrene at the DFTB vdw-D3 level.

Tetracene phonon band structure with c09-vdw-DF2 functional.

Numerical detail for electron-phonon coupling.

References

(1) Troisi, A.; Orlandi, G. Charge-Transport Regime of Crystalline Organic Semiconductors: Diffusion Limited by Thermal Off-Diagonal Electronic Disorder. *Phys. Rev. Lett.* **2006**, *96*, 0866011–0866014.

(2) Fratini, S.; Ciuchi, S.; Mayou, D.; de Laissardiere, G. T.; Troisi, A. A map of high-mobility molecular semiconductors. *Nat. Mater.* **2017**, *16*, 998–1002.

(3) Ortmann, F.; Bechstedt, F.; Hannewald, K. Charge transport in organic crystals: Theory and modelling. *Phys. Status Solidi B* **2011**, *248*, 511–525.

(4) Munn, R. W.; Silbey, R. Theory of electronic transport in molecular crystals. II. Zeroth order states incorporating nonlocal linear electron–phonon coupling. *J. Chem. Phys.* **1985**, *83*, 1843–1853.

(5) Lee, N.-E.; Zhou, J.-J.; Agapito, L. A.; Bernardi, M. Charge transport in organic molecular semiconductors from first principles: The bandlike hole mobility in a naphthalene crystal. *Phys. Rev. B* **2018**, *97*, 115203.

(6) Hannewald, K.; Stojanović, V. M.; Schellekens, J. M. T.; Bobbert, P. A.; Kresse, G.; Hafner, J. Theory of polaron bandwidth narrowing in organic molecular crystals. *Phys. Rev. B* **2004**, *69*, 0752111–0752117.

(7) Troisi, A.; Orlandi, G. Dynamics of the Intermolecular Transfer Integral in Crystalline Organic Semiconductors. *J. Phys. Chem. A* **2006**, *110*, 4065–4070.

(8) Fratini, S.; Mayou, D.; Ciuchi, S. The Transient Localization Scenario for Charge Transport in Crystalline Organic Materials. *Adv. Funct. Mater.* **2016**, *26*, 2292–2315.

(9) Wang, L.; Li, Q.; Shuai, Z.; Chen, L.; Shi, Q. Multiscale study of charge mobility of organic semiconductor with dynamic disorders. *Phys. Chem. Chem. Phys.* **2010**, *12*, 3309–3314.

(10) Coropceanu, V.; Cornil, J.; da Silva Filho, D. A.; Olivier, Y.; Silbey, R.; Brédas, J.-L. Charge transport in organic semiconductors. *Chem. Rev.* **2007**, *107*, 926–952.

(11) Troisi, A. Dynamic disorder in molecular semiconductors: Charge transport in two dimensions. *J. Chem. Phys.* **2011**, *134*, 0347021–03470210.

(12) Wang, L.; Beljonne, D. Flexible Surface Hopping Approach to Model the Crossover from Hopping to Band-like Transport in Organic Crystals. *J. Phys. Chem. Lett.* **2013**, *4*, 1888–1894.

(13) Wang, L.; Prezhdo, O. V.; Beljonne, D. Mixed quantum-classical dynamics for charge transport in organics. *Phys. Chem. Chem. Phys.* **2015**, *17*, 12395–12406.

(14) Chen, D.; Ye, J.; Zhang, H.; Zhao, Y. On the Munn−Silbey Approach to Polaron Transport with Off-Diagonal Coupling and Temperature-Dependent Canonical Transformations. *J. Phys. Chem. B* **2011**, *115*, 5312–5321.

(15) Mishchenko, A. S.; Nagaosa, N.; De Filippis, G.; de Candia, A.; Cataudella, V. Mobility of Holstein Polaron at Finite Temperature: An Unbiased Approach. *Phys. Rev. Lett.* **2015**, *114*, 1464011–1464015.

(16) Si, W.; Wu, C.-Q. Decoherence and energy relaxation in the quantum-classical dynamics for charge transport in organic semiconducting crystals: An instantaneous decoherence correction approach. *J. Chem. Phys.* **2015**, *143*, 0241031–0241037.

(17) Packwood, D. M.; Oniwa, K.; Jin, T.; Asao, N. Charge transport in organic crystals: Critical role of correlated fluctuations unveiled by analysis of Feynman diagrams. *J. Chem. Phys.* **2015**, *142*, 1445031–014450310.

(18) Heck, A.; Kranz, J. J.; Kubař, T.; Elstner, M. Multi-Scale Approach to Non-Adiabatic Charge Transport in High-Mobility Organic Semiconductors. *J. Chem. Theory Comput.* **2015**, *11*, 5068–5082.

(19) Oberhofer, H.; Blumberger, J. Revisiting electronic couplings and incoherent hopping models for electron transport in crystalline C60 at ambient temperatures. *Phys. Chem. Chem. Phys.* **2012**, *14*, 13846–13852.

(20) Eggeman, A. S.; Illig, S.; Troisi, A.; Sirringhaus, H.; Midgley, P. A. Measurement of molecular motion in organic semiconductors by thermal diffuse electron scattering. *Nat. Mater.* **2013**, *12*, 1045–1049.

(21) Illig, S.; Eggeman, A. S.; Troisi, A.; Jiang, L.; Warwick, C.; Nikolka, M.; Schweicher, G.; Yeates, S. G.; Henri Geerts, Y.; Anthony, J. E.; Sirringhaus, H. Reducing dynamic disorder in small-molecule organic semiconductors by suppressing large-amplitude thermal motions. *Nat. Commun.* **2016**, *7*, 107361–1073610.

(22) Kubo, T.; Häusermann, R.; Tsurumi, J.; Soeda, J.; Okada, Y.; Yamashita, Y.; Akamatsu, N.; Shishido, A.; Mitsui, C.; Okamoto, T.; Yanagisawa, S.; Matsui, H.; Takeya, J. Suppressing molecular vibrations in organic semiconductors by inducing strain. *Nat. Commun.* **2016**, *7*, 111561–111567.

(23) Venuti, E.; Bilotti, I.; Della Valle, R. G.; Brillante, A.; Ranzieri, P.; Masino, M.; Girlando, A. Polarized Raman Spectra of a Rubrene Single Crystal. *J. Phys. Chem. C* **2008**, *112*, 17416–17422.

(24) Munn, R. W.; Silbey, R. Theory of electronic transport in molecular crystals. III. Diffusion coefficient incorporating nonlocal linear electron–phonon coupling. *J. Chem. Phys.* **1985**, *83*, 1854–1864.

(25) Coropceanu, V.; Sánchez-Carrera, R. S.; Paramonov, P.; Day, G. M.; Brédas, J.-L. Interaction of charge carriers with lattice vibrations in organic molecular semiconductors: naphthalene as a case study. *J. Phys. Chem. C* **2009**, *113*, 4679–4686.

(26) Girlando, A.; Grisanti, L.; Masino, M.; Bilotti, I.; Brillante, A.; Della Valle, R. G.;

Venuti, E. Peierls and Holstein carrier-phonon coupling in crystalline rubrene. *Phys. Rev. B* **2010**, *82*, 0352081–0352088.

(27) Ordejón, P.; Boskovic, D.; Panhans, M.; Ortmann, F. *Ab initio* study of electron-phonon coupling in rubrene. *Phys. Rev. B* **2017**, *96*, 0352021–0352029.

(28) Motta, C.; Sanvito, S. Charge transport properties of durene crystals from first-principles. *J. Chem. Theory Comput.* **2014**, *10*, 4624–4632.

(29) Daniel, H.; Sriram, K.; J., M. A.; C., V. K. P. On the Nature of Nonplanarity in the [N]Phenylenes. *Chemistry – A European Journal 5*, 3399–3412.

(30) Jurchescu, O. D.; Meetsma, A.; Palstra, T. T. M. Low-temperature structure of rubrene single crystals grown by vapor transport. *Acta Crystallographica Section B* **2006**, *62*, 330–334.

(31) Elstner, M.; Porezag, D.; Jungnickel, G.; Elsner, J.; Haugk, M.; Frauenheim, T.; Suhai, S.; Seifert, G. Self−consistent−charge density−functional tight−binding method for simulations of complex materials properties. *Phys. Rev. B* **1998**, *58*, 7260–7268.

(32) Aradi, B.; Hourahine, B.; Frauenheim, T. DFTB+, a Sparse Matrix-Based Implementation of the DFTB Method. *J. Phys. Chem. A* **2007**, *111*, 5678–5684.

(33) Seifert, G.; Joswig, J. Density−functional tight binding: an approximate density−functional theory method. *Wiley Interdiscip. Rev. Comput. Mol. Sci.* **2012**, *2*, 456–465.

(34) Gaus, M.; Goez, A.; Elstner, M. Parametrization and Benchmark of DFTB3 for Organic Molecules. *J. Chem. Theory Comput.* **2013**, *9*, 338–354.

(35) Grimme, S.; Antony, J.; Ehrlich, S.; Krieg, H. A consistent and accurate ab initio parametrization of density functional dispersion correction (DFT−D) for the 94 elements H−Pu. *J. Chem. Phys.* **2010**, *132*, 1541041–15410419.

(36) Grimme, S.; Ehrlich, S.; Goerigk, L. Effect of the damping function in dispersion corrected density functional theory. *J. Comput. Chem.* **2011**, *32*, 1456–1465.

(37) Gaus, M.; Cui, Q.; Elstner, M. DFTB3: Extension of the Self-Consistent-Charge Density-Functional Tight-Binding Method (SCC-DFTB). *J. Chem. Theory Comput.* **2011**, *7*, 931–948.

(38) Witek, H. A.; Morokuma, K.; Stradomska, A. Modeling vibrational spectra using the self−consistent charge density−functional tight−binding method. I. Raman spectra. *J. Chem. Phys.* **2004**, *121*, 5171–5178.

(39) Witek, H. A.; Irle, S.; Morokuma, K. Analytical second−order geometrical derivatives of energy for the self−consistent−charge density−functional tight−binding method. *J. Chem. Phys.* **2004**, *121*, 5163–5170.

(40) Frisch, M. J.; Trucks, G. W.; Schlegel, H. B.; Scuseria, G. E.; Robb, M. A.; Cheeseman, J. R.; Scalmani, G.; Barone, V.; Mennucci, B.; Petersson, G. A.; Nakatsuji, H.; Caricato, M.; Li, X.; Hratchian, H. P.; Izmaylov, A. F.; Bloino, J.; Zheng, G.; Sonnenberg, J. L.; Hada, M.; Ehara, M.; Toyota, K.; Fukuda, R.; Hasegawa, J.; Ishida, M.; Nakajima, T.; Honda, Y.; Kitao, O.; Nakai, H.; Vreven, T.; Montgomery, J. A., Jr.; Peralta, J. E.; Ogliaro, F.; Bearpark, M.; Heyd, J. J.; Brothers, E.; Kudin, K. N.; Staroverov, V. N.; Keith, T.; Kobayashi, R.; Normand, J.; Raghavachari, K.; Rendell, A.; Burant, J. C.; Iyengar, S. S.; Tomasi, J.; Cossi, M.; Rega, N.; Millam, J. M.; Klene, M.; Knox, J. E.; Cross, J. B.; Bakken, V.; Adamo, C.; Jaramillo, J.; Gomperts, R.; Stratmann, R. E.; Yazyev, O.; Austin, A. J.; Cammi, R.; Pomelli, C.; Ochterski, J. W.; Martin, R. L.; Morokuma, K.; Zakrzewski, V. G.; Voth, G. A.; Salvador, P.; Dannenberg, J. J.; Dapprich, S.; Daniels, A. D.; Farkas, Ö.; Foresman, J. B.; Ortiz, J. V.; Cioslowski, J.; Fox, D. J. Gaussian 09 Revision D.01. Gaussian Inc. Wallingford CT 2013.

(41) Kunc, K.; Martin, R. M. *Phys. Rev. Lett.* **1982**, *48*, 406–409.

(42) Yi, Y.; Coropceanu, V.; Brédas, J.-L. Nonlocal electron-phonon coupling in the pentacene crystal: Beyond the Gamma-point approximation. *J. Chem. Phys.* **2012**, *137*, 1643031–1643036.

(43) Medrano Sandonas, L.; Teich, D.; Gutierrez, R.; Lorenz, T.; Pecchia, A.; Seifert, G.; Cuniberti, G. Anisotropic Thermoelectric Response in Two-Dimensional Puckered Structures. *J. Phys. Chem. C* **2016**, *120*, 18841–18849.

(44) Shang, H.; Carbogno, C.; Rinke, P.; Scheffler, M. Lattice dynamics calculations based on density-functional perturbation theory in real space. *Comput. Phys. Commun.* **2017**, *215*, 26–46.

(45) Abdulla, M.; Refson, K.; Friend, R. H.; Haynes, P. D. A first-principles study of the vibrational properties of crystalline tetracene under pressure. *J. Phys. Condens. Matter* **2015**, *27*, 3754021–37540210.

(46) Giannozzi, P.; Baroni, S.; Bonini, N.; Calandra, M.; Car, R.; Cavazzoni, C.; Ceresoli, D.; Chiarotti, G. L.; Cococcioni, M.; Dabo, I.; Dal Corso, A.; de Gironcoli, S.; Fabris, S.; Fratesi, G.; Gebauer, R.; Gerstmann, U.; Gougoussis, C.; Kokalj, A.; Lazzeri, M.; Martin-Samos, L.; Marzari, N.; Mauri, F.; Mazzarello, R.; Paolini, S.; Pasquarello, A.; Paulatto, L.; Sbraccia, C.; Scandolo, S.; Sclauzero, G.; Seitsonen, A. P.; Smogunov, A.; Umari, P.; Wentzcovitch, R. M. QUANTUM ESPRESSO: a modular and open-source software project for quantum simulations of materials. *J. Phys. Condens. Matter* **2009**, *21*, 3955021–39550219.

(47) Xie, Y.; Zheng, J.; Lan, Z. Full-dimensional multilayer multiconfigurational time-dependent Hartree study of electron transfer dynamics in the anthracene/C60 complex. *J. Chem. Phys.* **2015**, *142*, 0847061–08470613.

(48) Troisi, A. Prediction of the Absolute Charge Mobility of Molecular Semiconductors: the Case of Rubrene. *Adv. Mater.* **2007**, *19*, 2000–2004.

(49) Sánchez-Carrera, R. S. Theoretical characterization of charge transport in organic molecular crystals. Ph.D. thesis, Georgia Institute of Technology, 2008.

(50) Watanabe, M.; Chang, Y. J.; Liu, S.-W.; Chao, T.-H.; Goto, K.; Islam, M. M.; Yuan, C.-H.; Tao, Y.-T.; Shinmyozu, T.; Chow, T. J. The synthesis, crystal structure and charge-transport properties of hexacene. *Nat. Chem.* **2012**, *4*, 574–578.

(51) Nakayama, Y.; Uragami, Y.; Machida, S.; Koswattage, K. R.; Yoshimura, D.; Setoyama, H.; Okajima, T.; Mase, K.; Ishii, H. Full picture of valence band structure of rubrene single crystals probed by angle-resolved and excitation-energy-dependent photoelectron spectroscopy. *Appl. Phys. Express* **2012**, *5*, 1116011–1116013.

(52) Aghtar, M.; Liebers, J.; Strümpfer, J.; Schulten, K.; Kleinekathöfer, U. Juxtaposing density matrix and classical path-based wave packet dynamics. *J. Chem. Phys.* **2012**, *136*, 2141011–2141019.

(53) Li, Y.; Coropceanu, V.; Brédas, J.-L. Nonlocal electron-phonon coupling in organic semiconductor crystals: The role of acoustic lattice vibrations. *J. Chem. Phys.* **2013**, *138*, 2047131–2047136.

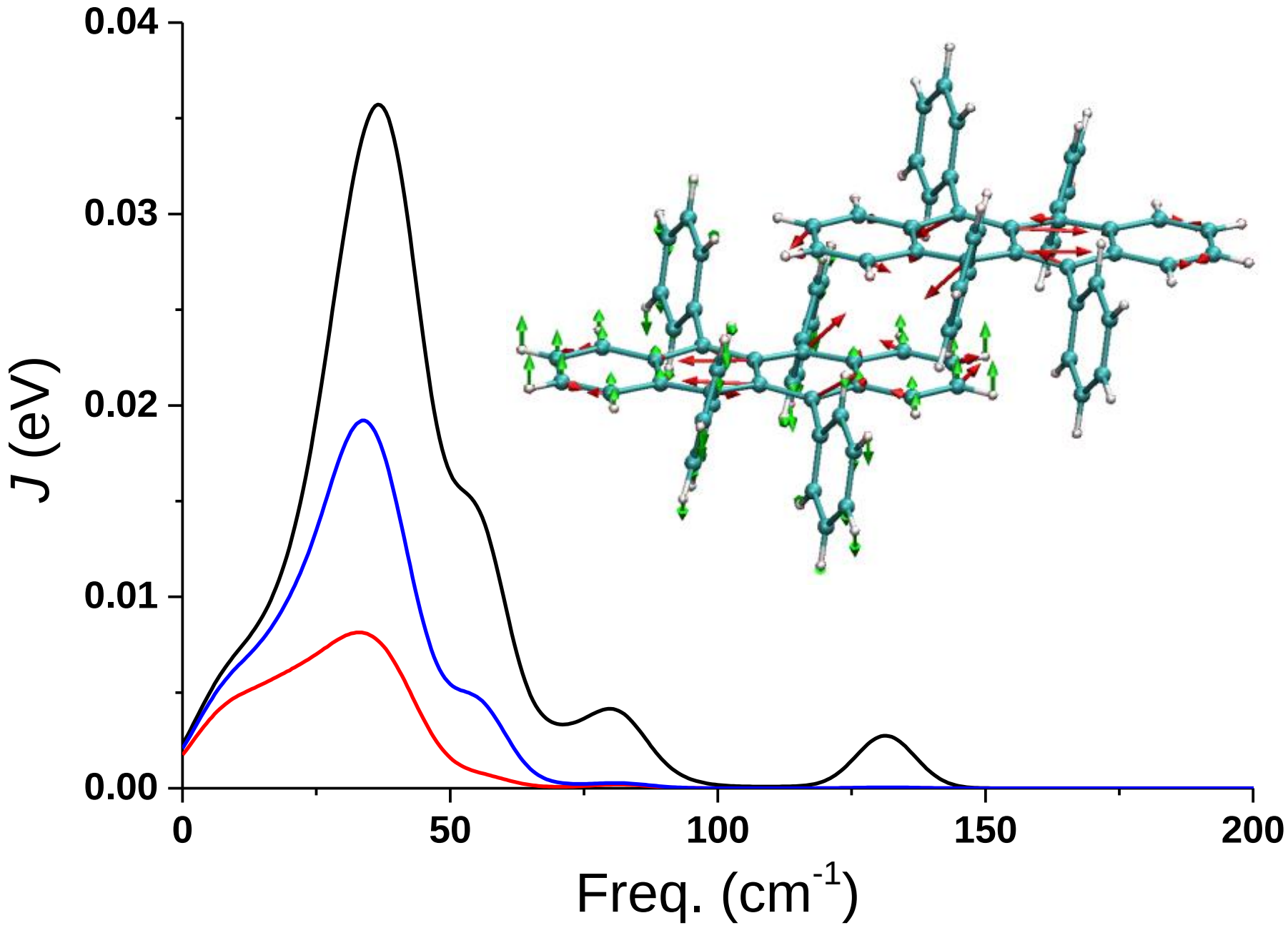
0.04
0.03
0.02
0.01
0.00
J (eV)
0
50
100
150
200
Freq. (cm-1)